IEEE Access
Multidisciplinary | Rapid Review | Open Access Journal

Received 4 October 2023, accepted 30 October 2023, date of publication 7 November 2023, date of current version 13 November 2023.

Digital Object Identifier 10.1109/ACCESS.2023.3330810

RESEARCH ARTICLE

Design and Experimental Validation of Permanent Magnet Motor for Propeller Aerodynamic Noise Test

HU YU[1], YONG-HUI CHEN[2], LIANG SUN[3], YONG ZHOU[1], AND ZHONG-REN WANG[4]

[1]Wuhan Institute of Marine Electric Propulsion, Wuhan 430064, China
[2]Aircraft Strength Research Institute, Xi'an 710065, China
[3]Hong Kong Centre for Cerebro-cardiovascular Health Engineering, City University of Hong Kong, Hong Kong 999077, China
[4]School of Mechanical Engineering, Hubei University of Arts and Science, Xiangyang 441053, China

Corresponding author: Zhong-Ren Wang (xfu_wangzhongren@126.com)

This work was supported by the State Key Laboratory of Electromagnetic Energy.

ABSTRACT The aerodynamic noise test platform for a certain type of unmanned aerial vehicle (UAV) imposes strict requirements on the drive motor, demanding high torque, small diameter, and low vibration. Compared to DC motors and induction motors, permanent magnet motors have advantages in terms of torque and volume, making them well-suited to meet the platform's requirements. In response to the development needs of the test platform for the drive motor, this study systematically analyzes the key technologies that require special attention in the design process of the permanent magnet motor. Through proper electromagnetic design, structural design, cooling design, and vibration design, particularly by verifying the electromagnetic performance under rated load and weak magnetic conditions, a 180 kW permanent magnet motor was manufactured for experimental validation. The motor was successfully utilized for propeller aerodynamic noise testing. The experimental results demonstrate that the 180kW permanent magnet motor meets the technical requirements of the test platform, confirming the accuracy of the permanent magnet motor design methodology. It provides a valuable reference for the design of similar propeller drive motors and holds practical engineering significance.

INDEX TERMS Propeller, permanent magnet motor, electromagnetic design, structural design, cooling design, vibration design.

I. INTRODUCTION

The propeller is the earliest power device of aircraft [1], which has the advantages of low fuel consumption and high flight efficiency, and is widely used in green electric aircraft and unmanned aerial vehicles [2], [3], [4]. However, the high-intensity noise generated by the propeller will directly radiate to the aircraft body and the surrounding environment [5], which reduces the performance quality and the stealth of the aircraft, and it also produces a series of structural safety and airworthiness problems. How to develop a propeller with high aerodynamic efficiency and low noise is a long-term research topic in the aviation industry, and its research methods include simulation calculation and experimental tests. The experimental test can verify and correct the simulation results, and is also the main research means for the design and evaluation of the propeller aerodynamic performance and noise [6], [7], [8]. Generally, the wind tunnel test is used to simulate the conditions of the propeller in the atmospheric flow field and to measure the aerodynamic performance and noise of the propeller, so as to evaluate and optimize the aerodynamic performance of the propeller. However, the cost of wind tunnel tests is huge. Only a few research institutions such as China Aerodynamics Research & Development Center [9], [10] and Northwestern Polytechnical University [11], [12] have the research conditions, and due to the limitation of wind tunnel size, most of them carry out scaled paddle tests [12]. Considering the cost limitation and the size limitation

The associate editor coordinating the review of this manuscript and approving it for publication was Hassen Ouakad.

of the wind tunnel test, this paper proposes to establish a fast, efficient, and low-cost test platform in the semi-anechoic chamber for the initial development of the propeller. The propeller aerodynamic noise test platform [5] can test the propeller aerodynamic noise, study the effects of rotational speed and blade Angle on propeller aerodynamic noise, analyze the main components of propeller noise, and provide direction for blade noise reduction design.

The propeller aerodynamic noise test platform is mainly composed of a fixed platform, drive motor, tension measuring system, torque measuring system, sliding platform and other components, as shown in Figure 1. During the test, the inverter drives the motor, and the motor transmits the driving force to the propeller through the spindle and elastic coupling, and drives the propeller to rotate to simulate the actual operation. There is a tension sensor at the back of the motor to measure the axial tension when the propeller rotates, and a torque sensor on the spindle to measure the torque of the propeller. By controlling the variable pitch motor at the end of the propeller to change the blade angle, the tension and torque of the propeller can be changed, and the aerodynamic performance and noise characteristics of the propeller can be measured.

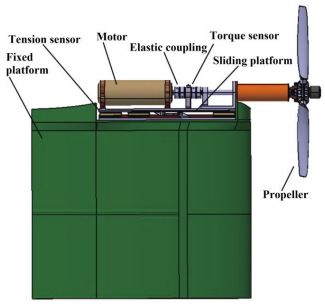

FIGURE 1. The propeller aerodynamic noise test platform.

The key component of the propeller aerodynamic noise test platform is the drive motor. To provide the drive torque required by the propeller rotation and reduce the interference of the drive motor's external size on the aerodynamic noise, the drive motor is required to have large torque, small outside diameter and low vibration. Compared with the commonly used DC motor and induction motor, the permanent magnet motor has the advantages of small size and high torque [13], [14], [15], and is suitable for the drive motor of the propeller aerodynamic noise test platform. In the previous design process of the propeller-driven motor, more attention was paid to electromagnetic design, structural design and cooling design [16], [17], [18], [19], [20], [21], [22], [23], [24], [25] to improve the power density of the drive motor, and little attention was paid to the vibration design of the drive motor. Due to the complicated structure, wide speed range and abundant vibration excitation sources of the permanent magnet motor, the vibration and noise characteristics of the permanent magnet motor are complex, and it is necessary to pay attention to the vibration design of the drive motor and the matching design with the propeller to ensure the smooth operation of the test platform. Based on this, a systematic design method for the drive motor is proposed from the aspects of electromagnetic, structure, cooling and vibration design, and it is used to develop the drive motor of the test platform. This design method can provide a reference for the design of similar test platform drive motors and other permanent magnet motors.

In this paper, a driving motor with high torque, small diameter, and low vibration is designed to be used as a propeller driver for the aerodynamic noise test of the UAV propeller. Firstly, the development requirements of the drive motor are introduced, and the key technologies of the drive motor design are analyzed. Secondly, it provides a detailed description of the design process for a permanent magnet motor, covering electromagnetic design, structural design, cooling design, and vibration design. Finally, a 180 kW permanent magnet motor is manufactured, and the correctness of the design method is verified by the motor test, and it is successfully used in the aerodynamic noise test of the UAV propeller.

II. DEVELOPMENT REQUIREMENTS AND KEY TECHNOLOGIES

A. DEVELOPMENT REQUIREMENTS OF THE DRIVE MOTOR

The aerodynamic noise test platform of a UAV propeller, as shown in Figure 2, needs to carry out an aerodynamic noise test of a reduced-scale propeller and a full-size propeller. According to the development requirements of a UAV [5], the speed and power requirements of the propeller are proposed, and then the corresponding speed and power requirements of the driving motor are proposed. According to the time that the propeller's aerodynamic noise test needs to achieve the stability of the propeller's operation, the corresponding running time requirements for the drive motor are put forward. To avoid the adverse effect on the atmospheric flow field caused by the excessively large outer diameter of the drive motor, and combined with the size of the propeller hub, the size requirements for the outer diameter of the drive motor are put forward. The cooling design requirements of permanent magnet motors are put forward in view of the demand for long-term tests of variable load driving motors. Considering the stable operation of the propeller test platform at high speed, the low vibration requirement of the permanent magnet motor is put forward. The technical requirements for the drive motor are as follows:

1) When the propeller speed is 2400 rpm, the motor drive power reaches 100 kW to meet the power demand of the full-size propeller;

2) When the propeller speed is 6500 rpm, the motor drive power reaches 180 kW to meet the power demand of the reduced scale propeller;

3) The single running time of the drive motor is not less than 30min;

4) The outer diameter size of the drive motor is not greater than 240 mm, and it is installed in the cylindrical fairing to

reduce the influence of external size on the aerodynamic noise of the propeller;

5) Drive motor heat dissipation requirements to meet long-term high power density output;

6) Low vibration requirements of the drive motor to reduce the interference of vibration on the accuracy of tensile and torque measurement.

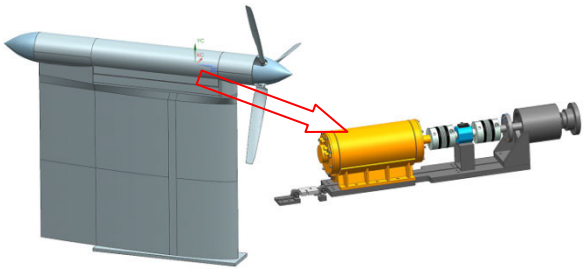

FIGURE 2. Aerodynamic noise test platform of a UAV propeller.

B. THE KEY TECHNOLOGY OF DRIVE MOTOR DESIGN

1) ELECTROMAGNETIC OPTIMIZATION DESIGN

Considering the speed and power requirements of the propeller to the drive motor, the maximum torque of the drive motor reaches 400 Nm; Considering the size requirements of the drive motor on the test platform, the outside diameter of the drive motor body is not greater than 240 mm. The torque requirements of the drive motor are large, and the diameter requirements are small, there is a certain contradiction between the two requirements, and it is necessary to coordinate this contradiction through electromagnetic design [26], [27], [28], [29], and by drawing on mature design experience and accurate calculation means to meet all technical requirements, which puts forward higher requirements for the electromagnetic design of the drive motor.

The torque of a permanent magnet motor is generated by the interaction between the stator armature magnetic field and the rotor magnetic field, and the size parameters to be determined in its electromagnetic design are mainly the punching and permanent magnet size related to the magnetic circuit and the winding parameters related to the circuit. The electromagnetic design mainly adopts the method of combining field and circuit, gives the initial design scheme according to the design input requirements and previous design experience, then calculates the performance index of the given design scheme through the finite element method, and adopts the optimization algorithm such as genetic algorithm and Taguchi algorithm according to the calculation results to adjust and improve the design scheme, and finally meets the design requirements.

2) EFFICIENT COOLING DESIGN

For the heat dissipation requirements of the high power density drive motor, due to the strict requirements of the test platform on the torque and outside diameter of the drive motor, the electromagnetic load of the drive motor is increased, and the drive motor is installed in the inside of the fairing, which will lead to more serious heating and temperature rise, and it is necessary to do an efficient cooling design [30], [31], [32], [33] of the drive motor.

The cooling of the motor is generally divided into natural cooling, gas forced cooling and liquid forced cooling [16]. Due to the large torque and small outside diameter of the motor, and the motor installed inside the fairing, natural cooling and gas-forced cooling is usually difficult to meet the heat dissipation requirements. For liquid forced cooling, water cooling or oil cooling is generally used, although the oil cooling effect is good, the cooling oil circuit needs to use a dynamic seal, and needs to be equipped with a special oil station, the cooling system is complex and difficult to process, not suitable for the drive motor which mounted inside the fairing, therefore, the drive motor is intended to use water cooling.

The usual structure of water cooling is the stator frame water cooling structure. The frame is set in the spiral or axial waterway, and the frame and the iron core adopt an interference fit, which has a good cooling effect on the stator iron core, but a weak cooling effect on the stator winding and rotor. Therefore, for the drive motor with high power density, it is necessary to carry out cooling calculations in various operating conditions to check whether the temperature rise limit is exceeded. The temperature distribution is calculated to guide the efficient cooling design of the motor.

3) MATCHING DESIGN OF ELECTROMAGNETIC EXCITATION CHARACTERISTICS AND STRUCTURAL VIBRATION CHARACTERISTICS

For the low vibration requirements of the drive motor, because the vibration of the drive motor is mainly generated by electromagnetic excitation, it is necessary to pay attention to the coupling resonance between the electromagnetic excitation characteristics and the structural vibration characteristics [34], [35], [36], [37].

The electromagnetic exciting force of a permanent magnet motor is mainly the electromagnetic wave that changes with time and space due to the interaction of stator and rotor magnetic field in the air gap magnetic field, including radial force wave (radial electromagnetic exciting force) and tangential force wave (cogging torque and torque ripple, etc.). It is generally believed that radial force wave is the main excitation that causes vibration, and its electromagnetic force frequency has typical spatial characteristics. The modes of spatial order 2 and 4 are shown in Figure 3.

The structural vibration characteristics of permanent magnet motors need to pay attention to the stator structural modal, which has the vibration characteristics of typical cylindrical structures, as shown in Figure 4, and is easy to resonate with electromagnetic excitation force in frequency and modal shape. Therefore, in the process of stator structure design, it is necessary to calculate the modal frequency of the sta-

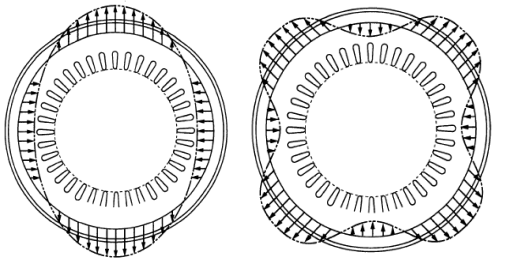

FIGURE 3. Typical spatial characteristics of electromagnetic excitation force.

tor structure, and compare and analyze the electromagnetic excitation frequency under the main operating conditions of the motor, to avoid resonance in frequency and modal shape. If there is resonance, the electromagnetic excitation frequency under the main operating conditions of the motor is avoided by optimizing the structure size of the stator core yoke and the stator frame.

In addition, it is also necessary to consider the vibration caused by the coupling of the electromagnetic frequency of the motor and the blade frequency of the propeller. Select the appropriate number of motor poles and slots in the design, so that the electromagnetic excitation frequency of the motor and the blade frequency of the propeller are completely staggered, and there is no coupling resonance, to ensure the normal operation of the equipment.

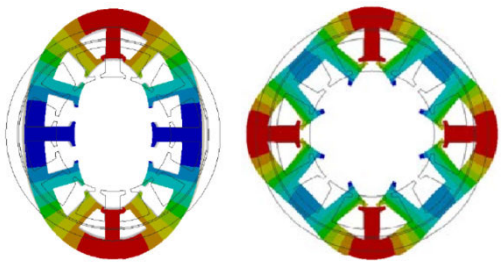

FIGURE 4. Typical vibration mode of the stator core.

III. PERMANENT MAGNET MOTOR DESIGN

A. MOTOR DESIGN PROCESS

The design of the propeller aerodynamic noise test platform with a permanent magnet drive motor is constrained by the structural dimensions. It requires considering the performance aspects of electromagnetic, structural, cooling, and vibration factors. The design process involves iterative coupling of various physical parameters, as shown in Figure 5. Under given design input conditions, initial selections are made for thermal load, magnetic load, and optimization of pole slot fit parameters to determine the basic electromagnetic structural parameters. Based on this, finite element simulation calculations are carried out to evaluate electromagnetic performance. If the design requirements are met, necessary analyses and calculations are conducted for structural, cooling, and vibration aspects until the design requirements are satisfied. It can be observed that the design of the permanent magnet drive motor involves aspects such as electromagnetic, structural, cooling, and vibration considerations, with electromagnetic design being fundamental and requiring particular attention.

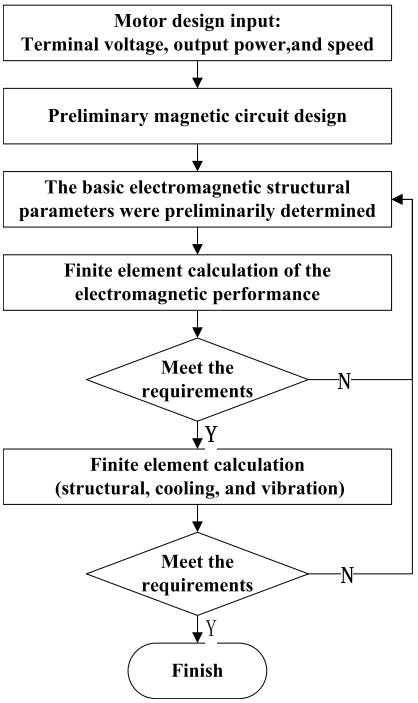

FIGURE 5. Motor design process flowchart.

B. ELECTROMAGNETIC DESIGN

1) BASIC PARAMETERS AND STRUCTURE OF THE MOTOR

According to the development requirements of the drive motor, the rated speed of the motor is 4297 rpm, the speed range of 0∼4297 rpm is 400 Nm constant torque operation, and the speed range of 4297∼6500 rpm is 180 kW constant power operation.

Considering that the speed and operating conditions of the motor require a certain weak magnetic debugging ability, the motor adopts a "V+ one" embedded rotor structure. According to the electromagnetic design method of the permanent magnet motor, the main structural parameters of the 180 kW permanent magnet motor can be determined after preliminary magnetic circuit design, as shown in Table 1. The motor structure and stator groove shape are shown in Figure 6. The rotor adopts the "V+ one" embedded structure, which is characterized by the rotor's quadrature axis reactance being much higher than the direct axis reactance, which can make full use of the reluctance torque of the motor. At the same time, the built-in rotor magnetic circuit structure not only easy to weak magnetic expansion, but also the magnetic leakage coefficient is larger than that of the surface rotor, which helps

to improve the anti-demagnetization ability of the motor and ensure the reliability and stability operation of the permanent magnet.

To reduce the low harmonics of the motor, the stator adopts a short-moment winding with the number of slots per pole per phase is 2 and a span is 5. The stator and rotor silicon steel sheet adopts 35DW250, because the motor has high-speed operating conditions and high frequency. The silicon steel sheet with low iron loss is selected to improve the temperature rise of the motor. The permanent magnet of the rotor is NdFeB 40UH, the reason is that considering the high temperature rise of the rotor, the use of UH grade can improve the temperature resistance of the magnetic steel, and NdFeB 40UH has high remanence, high coercivity, high magnetic energy product, and high-temperature resistance, and it is easy to process into various shapes and sizes, especially suitable for high power and high magnetic field.

TABLE 1. The main parameters of the 180kW permanent magnet motor.

Parameter	Value
Rated power/kW	180
Efficiency	0.96
Rated speed/rpm	4297
Frequency/Hz	286.467
Line voltage/V	350
Phase current/A	339.73
Number of poles	8
Phase	3
Number of stator slots	48
Number of conductors per slot	12
Stator outer diameter (mm)	210
Stator inner diameter/mm	145
Air gap length/mm	1.2
Core axial length/mm	391
The fundamental amplitude of gap flux density/T	0.8
Number of parallel branches	8
Wire diameter	10×ϕ0.71
Permanent magnet size/mm	21.4×4.0

2) MOTOR MODEL AND BOUNDARY EQUIVALENCE

Due to the periodic symmetry of the motor structure, a pair of motor poles is taken as the solution domain and treated as follows:

(a) The magnetic field is unchanged along the axis, the magnetic field in the permanent magnet motor is treated as a two-dimensional field. Meanwhile, in order to improve the accuracy of the calculation, the influence of the end effect on the motor voltage [38], [39] is taken into account by the end leakage inductance and end resistance in the winding circuit equation, as shown in Figure 7, where LA1 represents the inductance of phase A1, Le represents the end leakage inductance of each phase winding, and Ra indicates the resistance of each phase winding;

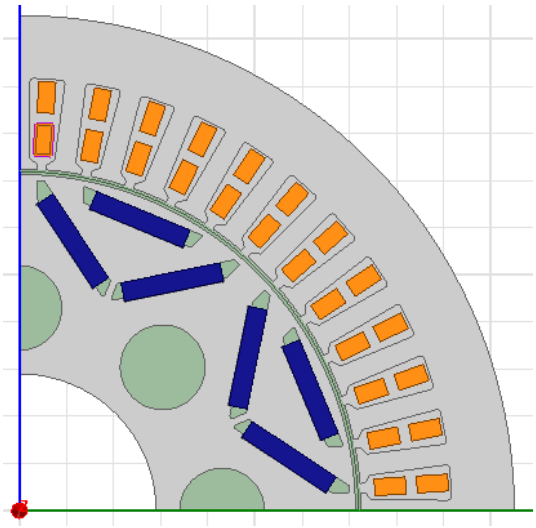

FIGURE 6. A pair of poles structure of permanent magnet motor.

(b) Ignore the magnetic leakage of the outer circle of the stator frame;

(c) Ignoring the hysteresis effect of ferromagnetic materials.

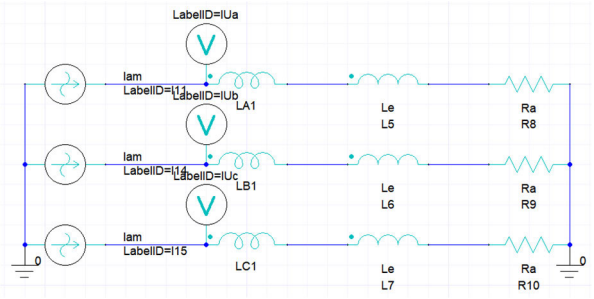

FIGURE 7. Equivalent external circuit diagram of the motor.

3) NO-LOAD CALCULATION

The no-load calculation is to specifies the no current in the subwinding, and only the permanent magnet acts alone. The average operating temperature of the magnetic steel is 100 °, and the motor speed is 4297 r/min. The flux density distribution of each part of the motor can be determined through no-load calculation, which provides a basis for the subsequent calculation of iron loss. The computed cloud map of no-load flux density distribution is shown in Figure 8 and the distribution characteristics of magnetic density can be seen. The flux density of each part is smaller than the saturation flux density of the silicon steel sheet, and the flux density meets the design requirements. The rotor magnetic bridge has a local saturation point, but the area is small, and the magnetic field in the rotor is small, and the loss can be almost ignored. The flux density distribution of each part of the motor is shown in Table 2, which can be used as input parameters for subsequent iron consumption calculation.

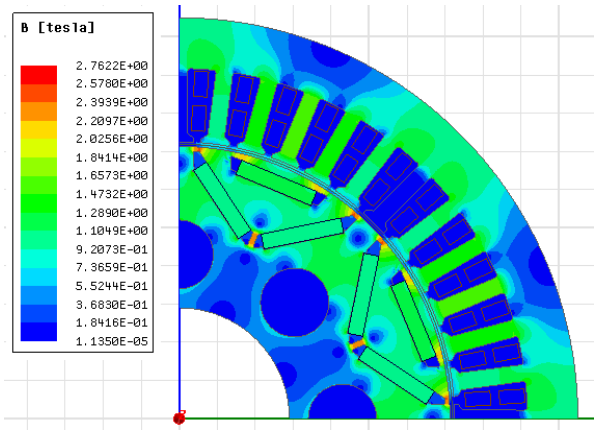

FIGURE 8. Flux density distribution of no-load condition.

TABLE 2. Flux density values of each part.

Parameter	Value
The fundamental amplitude of air gap flux density/T	0.82
The flux density of the stator teeth/T	1.54
The flux density of stator yoke/T	1.20
The flux density of rotor yoke/T	1.32

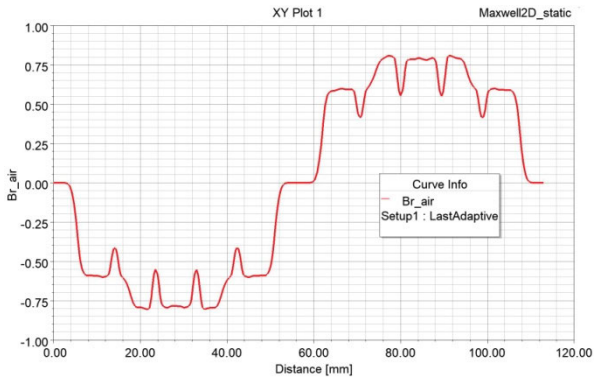

FIGURE 9. The radial component waveform of air gap flux density.

The radial component waveform of the flux density at the center of the air gap is shown in Figure 9. Due to the influence of the stator slot and rotor pole shape, harmonic components are abundant, especially the third, fifth, and seventh harmonics, and tooth harmonics are obvious, which can be weakened by winding short distance, distribution, and stator slot or rotor oblique pole. The use of inclined slots or inclined poles needs to be selected according to the complexity of the process. In this paper, the use of inclined slots can better optimize the air gap magnetic density and back potential waveform.

After the skewed slot, the calculated back electromotive force curve with time is shown in Figure 10. The harmonic content of the motor is greatly reduced, and the waveform distortion rate of the back electromotive force of the motor is only 1.18%.

4) CALCULATION OF RATED LOAD CONDITION

The rated load is calculated with the current source as input, and the stator winding is loaded with sinusoidal phase current with an amplitude of 480.45 A. The axial length of the motor satisfying the three performance parameters of rated voltage, rated electromagnetic torque and rated power factor is obtained by several scanning and iterative calculations through the internal power factor Angle. During calculation, the stator winding is set according to the working temperature of 100 °C, and the load flux density distribution is shown in Figure 11. The flux density of each part of the stator and rotor is still less than the saturation flux density of the silicon steel sheet, which can make full use of the magnetic permeability and reduce iron consumption.

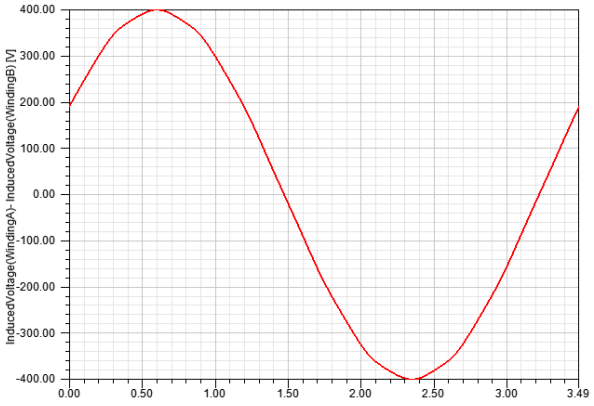

FIGURE 10. Line back electromotive force wave of no-load condition.

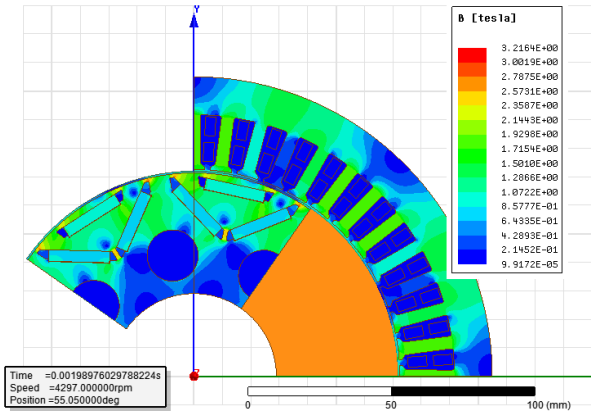

FIGURE 11. Flux density distribution of load.

In the electromagnetic calculation process, the current source is used for excitation loading, and the simulation results are directly run to a stable state. The electromagnetic torque waveform obtained by calculation is shown in Figure 12. Due to the use of current source excitation, the simulation results run directly to a stable state, reaching the rated torque requirement of 400 Nm. Although there is a certain fluctuation in torque, the torque fluctuation is less than 5%, which has less impact on the vibration and noise

of the motor. The load performance is shown in Table 3. The voltage, power factor, and electromagnetic torque all meet the design requirements.

Under the rated load, according to the corresponding calculation formula of copper loss, iron loss and mechanical loss, and according to the flux density of each part in Table 2, the loss of each part of the motor is calculated as shown in Table 4. The table will be used as input for the thermal calculation of the motor.

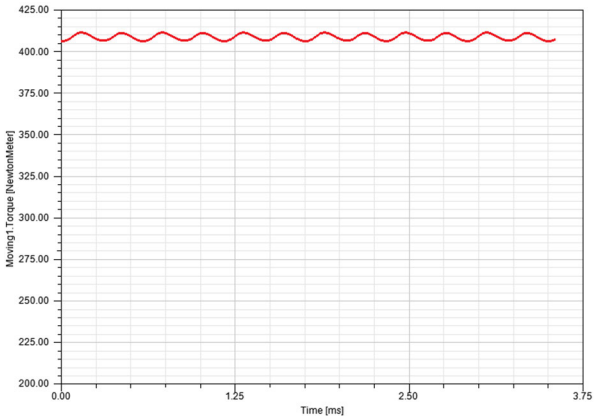

FIGURE 12. Electromagnetic torque waveform of the load condition.

TABLE 3. Performance of load condition.

Parameter	Value
Phase current/A	340
Internal power factor Angle	34.5
The amplitude of the phase voltage/V	344
Power factor	0.94
Electromagnetic torque/Nm	412

TABLE 4. Loss at rated load conditions.

Parameter	Value
Copper loss in slot winding/kW	2.870
Copper loss at end winding/kW	0.766
Iron loss at core teeth/kW	1.186
Iron loss at core yoke/kW	1.152
Wind and mechanical friction loss/kW	0.500

5) FLUX-WEAKENING CONTROL CALCULATION

To ensure that the rated sinusoidal current value is unchanged, the internal power factor angle is adjusted to achieve the purpose of 180 kW constant power flux-weakening speed up to 6500 r/min. At this speed, the back potential of the motor will exceed the end voltage, and it is necessary to use weak magnetic control to meet the requirements of the end voltage. After the flux-weakening control is adopted, the calculated phase voltage is shown in Figure 13, and it is within the allowable range of the rated voltage. The electromagnetic torque waveform is shown in Figure 14, which can reach the power requirement of 180 kW. The weak magnetic properties are shown in Table 5, and the internal power Angle increases from 34.5 to 65.7 degrees, indicating that the demagnetization component of the motor is greatly increased, and the torque component is greatly reduced, but the total torque still meets the design requirements.

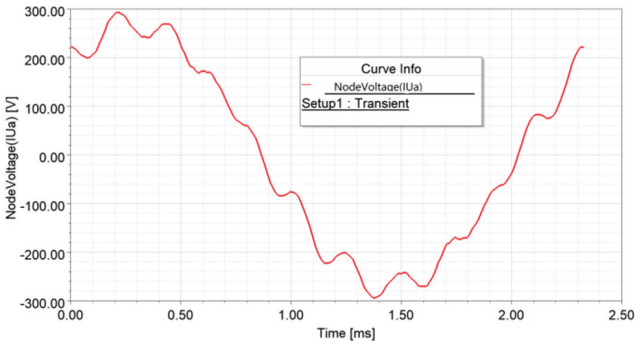

FIGURE 13. Phase voltage waveform at 6450 r/min.

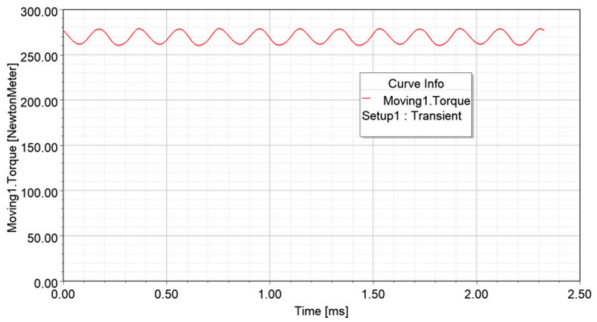

FIGURE 14. Electromagnetic torque waveform at 6450 r/min.

TABLE 5. Performance of flux-weakening condition.

Parameter	Value
Phase current/A	336
Internal power factor Angle	65.7
The amplitude of the phase voltage/V	334
Power factor	0.96
Electromagnetic torque/Nm	268

6) CALCULATION OF THE WORKING CURVE

Considering that the motor has speed regulation requirements, the maximum torque and speed curves of the motor at different speeds were analyzed and calculated under the given maximum current of 340 A and busbar voltage of 495V, as shown in Figure 15. The motor runs at a constant torque

of 400Nm in the speed range of 0∼4297 r/min, achieving the design requirement of power not less than 100 kW at the speed of 2400 r/min. The motor runs at constant power in the speed range of 4297∼6450 r/min, and the power is not less than 180kW when the speed is 6500 r/min. All of them meet the technical requirements.

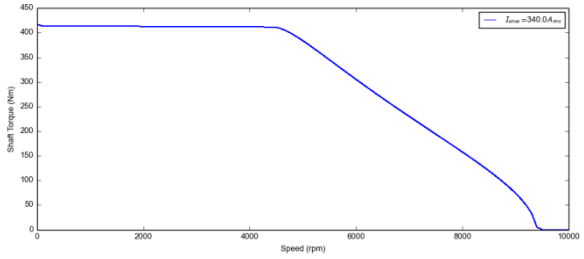

FIGURE 15. The relationship between the maximum output torque and speed of the motor at the rated current of 340A.

The efficiency MAP of the motor under different speeds and torque is shown in Figure 16. The efficiency is above 96% in the range of operating conditions, and the design performance of the permanent magnet motor is good.

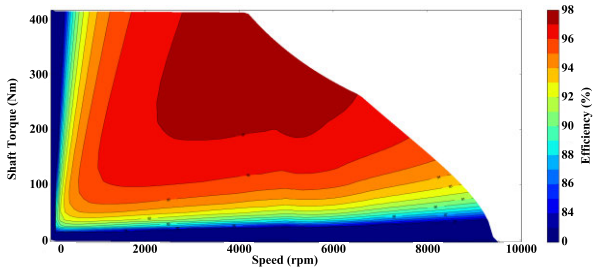

FIGURE 16. The efficiency MAP of the motor at different speeds and torques.

C. STRUCTURAL DESIGN

1) STATOR STRUCTURE DESIGN

The stator mainly includes a stator core, a stator winding, a frame, an end cover and a front and rear water collector. The stator structure is shown in Figure 17. The stator frame is made of aluminum alloy, and the cooling water tank is opened in the axial direction, which passes water to cool the motor. The frame and the water collector are welded into a whole to form a complete waterway, and the inlet and outlet are on the front and rear water collectors, and are connected with the outside through the hose. The motor foot and the water cooling frame are welded into a whole.

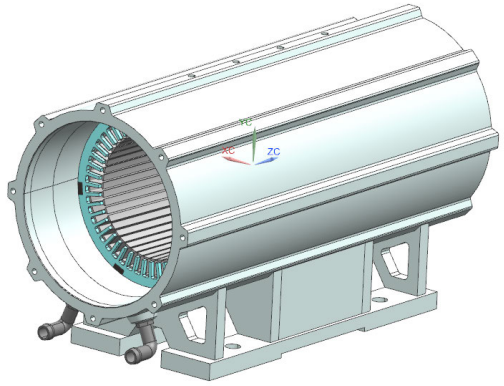

FIGURE 17. Motor stator structure.

The stator core is superimposed by a round punching, and the dovetail groove is arranged on its back. After superimposed, six buckle slabs are used to tighten and weld firmly. The stator winding adopts loose line overlapping winding, the insulation adopts an H-class insulation structure, and the outgoing wire exits directly from the non-drive end cover. A total of six PT100 temperature sensors are embedded in the stator slot and the end-winding where the heat is most severe, among which three are in the slot and three are in the end-winding to protect the motor from overheating.

2) ROTOR STRUCTURE DESIGN

The rotor is mainly composed of a rotating shaft, rotor core, magnetic steel and position sensor components, and the rotor structure is shown in Figure 18. The rotor is excited by the NdFeb permanent magnet and adopts an embedded magnetic pole structure. The structure of the magnetic pole is segmented along the axial direction. The silicon steel sheet is formed into a whole with rivets, and is inserted into the shaft through a hot sleeve, The magnetic steel is pushed in along the axial direction, and the anaerobic glue is applied before the pushing in. Both ends are fixed with baffles and finally locked with locking nuts. Balance blocks can be added at both ends of the baffle to meet the requirements of dynamic balance. The position sensor uses a rotating transformer and is fixed at the non-drive end shaft extension.

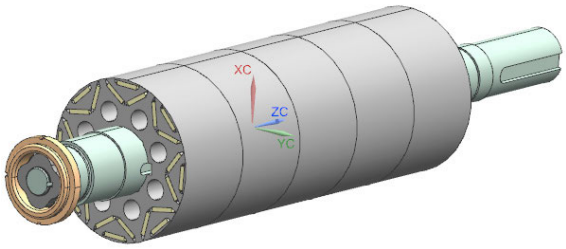

FIGURE 18. Motor rotor structure.

D. COOLING DESIGN

1) THE COOLING MODE

The permanent magnet motor adopts the water-cooling method, and the cooling tank is arranged outside the frame. The cooling structure is shown in Figure 19.

For the cooling of the stator core and winding, the loss mainly includes copper loss and iron loss, which are radially transmitted to the teeth and yoke of the core, and then transmitted to the cooling water of the frame tank, which is carried away in the form of convection.

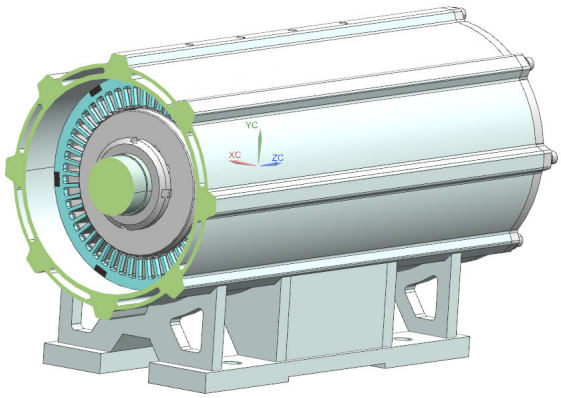

FIGURE 19. The cooling structure of the permanent magnet motor.

For the cooling of the end-winding, the heat generated is transmitted axially to the core winding and taken away by the cooling water of the stator frame.

For the cooling of the rotor, the rotor loss is mainly the pulsation loss at the magnetic pole surface, and the electromagnetic calculation results show that the loss value is small. The heat generated can be transmitted to the rotating shaft, the gap air and the air inside the rotor, and finally taken away by the outside air to achieve the cooling of the rotor. The gap air can isolate the heat of the main heating stator part from the rotor area, so that the permanent magnet can work safely and reliably.

2) TEMPERATURE RISE CALCULATION UNDER RATED WORKING CONDITIONS

The initial cooling water flow is 12.4 L/min, and the initial temperature is 30 °C. The radial and axial temperature distributions under rated working conditions can be obtained by the thermal circuit calculation. The highest temperature is mainly distributed at the end winding, as shown in Figure 20.

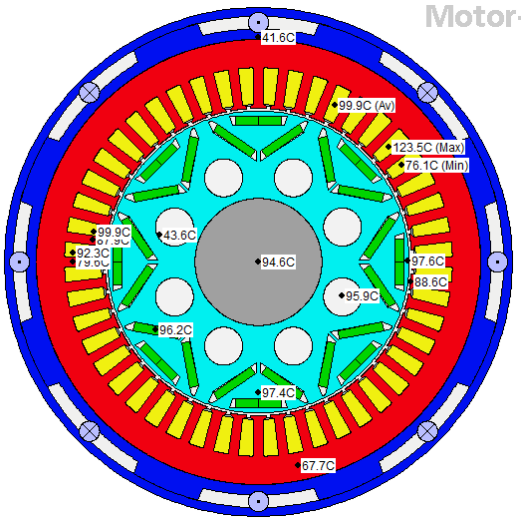

FIGURE 20. Radial temperature distribution at rated load conditions.

The temperature rise of each part of the motor is shown in Table 6, and the temperature rise meets the assessment requirements of H-class (180 °C) insulation.

TABLE 6. Comparison of temperature rise of each part.

Item	Maximum temperature/°C	Temperature rise/K
Core segment winding	99.9	69.9
End winding	123.5	93.5
Stator tooth	88.6	58.6
Stator core yoke	67.7	37.7
Rotor pole	96.2	66.2

3) TEMPERATURE RISE CALCULATION UNDER FLUX-WEAKENING CONDITION

The initial cooling water flow rate was set at 12.4 L/min, with an initial temperature of 30 °C. Using thermal analysis, the radial and axial temperature distributions of the motor under weak magnetic conditions were calculated. The highest temperatures were mainly observed at the end-winding positions, as shown in Figure 21. Under weak magnetic conditions, the increased motor speed resulted in higher mechanical friction losses due to windage on the rotor surface and bearing friction, leading to a significant temperature rise in the rotor. The maximum temperature on the magnet surface reached up to 114 °C, but it is still within the permissible operating temperature range.

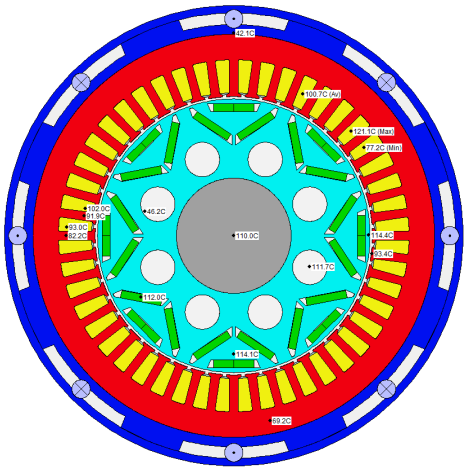

FIGURE 21. Radial temperature distribution under flux-weakening conditions.

According to the thermal calculation of the permanent magnet motor, the stator components and rotor poles are always under the safe operating temperature under rated operating conditions and flux-weakening operating conditions, which meets the design requirements, and the motor cooling scheme is reasonable and feasible.

E. VIBRATION DESIGN

1) ELECTROMAGNETIC EXCITATION FREQUENCY CALCULATION

The permanent magnet drive motor [16] used in a wind tunnel test for a scaled paddle has a rated power of 80 kW, a rated

torque of 115 Nm, a rated speed of 6600 rpm, and a maximum speed of 8500 rpm. Compared with the 80 kW permanent magnet drive motor, the torque and power of the motor in this paper are larger, and the vibration will be also larger. At the same time, because the drive motor is installed on the slide of the test platform, more attention needs to be paid to the vibration design of the motor.

The electromagnetic vibration frequency of the drive motor should avoid the blade frequency generated by the propeller rotation, so as to reduce the influence of the drive motor vibration on the aerodynamic performance and noise characteristics of the propeller. Because the propeller is a three-blade propeller, its blade frequency is related to the speed and number of blades, so the pole number of the permanent magnet motor is set to 8, to avoid the coupling of the propeller blade frequency and the electromagnetic excitation frequency of the motor.

According to the speed, the number of poles and the number of slots, the power fundamental wave frequency, main wave electromagnetic force frequency and tooth harmonic frequency of the permanent magnet motor can be calculated under the main operating conditions. According to the rotation speed of the propeller and the number of blades, the blade frequency of the propeller can be calculated, as shown in Table 7. It can be seen that the electromagnetic excitation frequency of the motor and the blade frequency of the propeller are completely staggered, and they will not produce coupling resonance, thus ensuring the normal operation of the equipment.

TABLE 7. Electromagnetic characteristic frequency and propeller blade frequency.

Item	2400 rpm	6500 rpm
Fundamental frequency of power supply/Hz	160.0	433.3
Main wave electromagnetic force frequency/Hz	320.0	866.7
Tooth harmonic frequency/Hz	1920.0	5200.0
The rotation frequency of the motor/Hz	40.0	108.3
Blade frequency of propeller/Hz	120.0	325.0

2) STRUCTURAL MODAL CALCULATION

According to the three-dimensional geometric model of the 180 kW permanent magnet motor, as shown in Figure 22, the structural equivalent model is established in the finite element software, including the structural components of the stator core, the stator frame and the end cover. The rotor is applied to the support of the end cover in the form of concentrated mass, and the stator winding is applied to the teeth of the stator core in the form of distributed mass.

For the 180 kW permanent magnet motor, the electromagnetic excitation force acting on the stator teeth changes with time and space is the main contribution of the motor vibration. Because the stator core of the conventional circular structure has the vibration characteristics of a typical

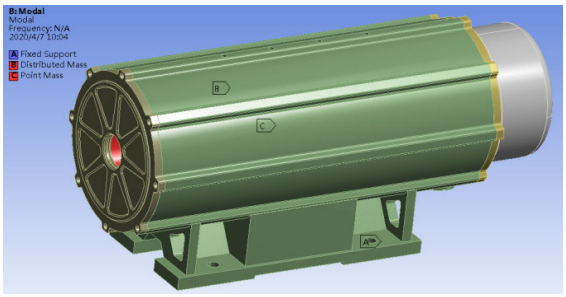

FIGURE 22. Structural calculation model of permanent magnet motor.

cylindrical structure, it is easy to have strong resonance with the electromagnetic excitation force in the frequency and modal shape. Therefore, it is necessary to pay attention to the matching design of the stator structure mode and electromagnetic excitation characteristics to avoid strong resonance.

The modal frequency calculation results of the stator structure of the permanent magnet motor are shown in Table 8. The modal calculation results show that: 1) the power fundamental wave frequency (158.7 Hz, 430.0 Hz) and main wave electromagnetic force frequency (317.3 Hz, 860.0 Hz) of the permanent magnet motor are far different from the radial polar order structure mode, and there will be no resonance in the working state. 2) The tooth harmonic frequency (1904.0 Hz, 5160.0 Hz) of the permanent magnet motor is far from the zero-order breathing mode, and will not resonate in the working state.

TABLE 8. Modal calculation results of the stator structure.

Number	Axial order	Radial order	The results of modal frequency calculation/Hz
1	0	2	970.7
2	0	2	1018.3
3	1	2	1126.0
4	1	2	1129.7
5	2	2	1994.6
6	2	2	2068.7
7	0	3	2349.5
8	0	3	2468.9
9	1	3	2537.4
10	1	3	2539.7
11	2	3	2843.4
12	2	3	2859.3
13	0	4	4643.9
14	0	4	4988.9
15	0	5	6013.7
16	0	5	6026.5

IV. PERMANENT MAGNET MOTOR TEST

A. BASIC PARAMETERS OF PERMANENT MAGNET MOTOR AND MODAL TEST OF THE STATOR STRUCTURE

According to the basic parameters of the motor mentioned above, the 180 kW permanent magnet motor is trial-produced, as shown in Figure 23. The maximum speed is 7000 rpm, the total length is 781 mm, the outside diameter of

FIGURE 23. The 180kW permanent magnet motor.

the motor frame is 240 mm, and the outside diameter of the shaft is 48 mm. The mass of the whole machine is 124 kg, and the power density is 1.45 kW/kg. It meets the requirements of the propeller aerodynamic noise test platform for motor dimensions.

During the manufacturing process of the 180 kW permanent magnet motor, modal tests were conducted using the impulse hammer method on the stator core, motor frame, and stator structure (Figure 24). The modal simulation calculations were performed based on previous research [36], considering the equivalent treatment of the stator core and windings. As a result, the modal simulation results were in good agreement with the modal test results (Table 9), with a relative error in modal frequencies within 5.1%. This verification confirms the accuracy of the modal calculations in this study.

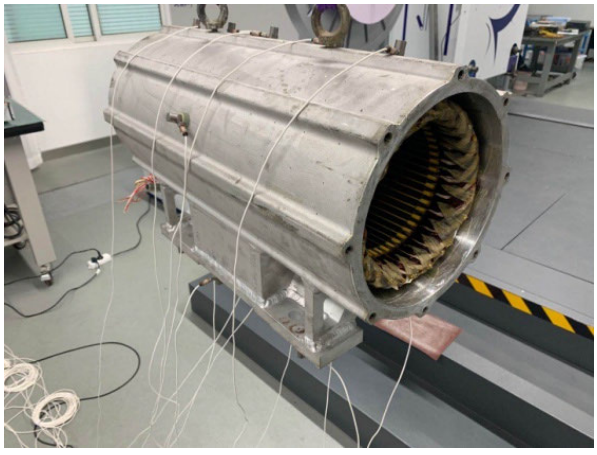

FIGURE 24. Modal test of the stator structure.

B. NO-LOAD BACK POTENTIAL TEST

The permanent magnet motor was initially driven by the prime mover and operated as a generator at no-load with a speed of 750 rpm in a cold state (Figure 25). The three-phase back EMF waveforms of the motor were simultaneously recorded using an oscilloscope, along with the ambient temperature. The measured no-load back EMF waveform at 750 rpm is shown in Figure 26. The magnitude and waveform of the no-load back EMF are determined by the

TABLE 9. Modal calculation results and modal test results of the stator structure.

Number	The results of calculation/Hz	The results of test/Hz	Relative error
1	970.7	976.1	0.5%
2	1018.3	/	/
3	1126.0	1095.0	2.8%
4	1129.7	1110.6	1.7%
5	1994.6	1927.8	3.5%
6	2068.7	1967.8	5.1%
7	2349.5	2320.4	1.3%
8	2468.9	2448.7	0.8%
9	2537.4	2505.0	1.3%
10	2539.7	2554.4	0.6%
11	2843.4	2748.0	3.5&
12	2859.3	2865.8	0.2%
13	4643.9	/	/
14	4988.9	/	/
15	6013.7	/	/
16	6026.5	/	/

electromagnetic design and can reflect the correctness of the electromagnetic scheme. Due to the adoption of distributed short-pitch windings in the stator, the 5th and 7th harmonic components in the air gap magnetic field are suppressed, resulting in an approximately sinusoidal waveform for the back EMF. The measured results align with the expected waveform.

Based on the measured back EMF of 72 V at 750 rpm, the back EMF at 4297 rpm can be calculated as 412.5 V. Considering the ambient temperature of 25 °C, the back EMF can be extrapolated to 100 °C, resulting in a value of 384.6 V. This value closely matches the calculated value of 387.6 V, validating the accuracy of the electromagnetic design.

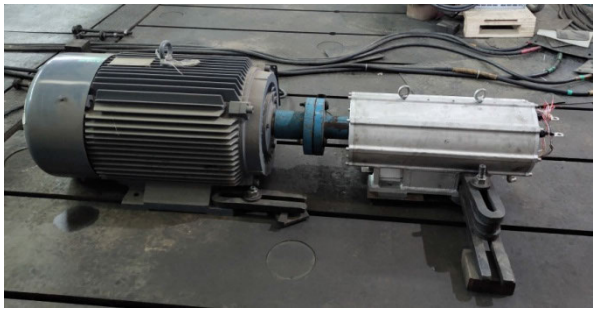

FIGURE 25. Back potential test site.

C. NO-LOAD RUNNING TEST OF MOTOR

On the cast iron platform of the laboratory, the no-load operation test of the permanent magnet motor at different speeds was carried out. The test site layout is shown in Figure 27. The maximum speed of the motor could reach 7000 rpm, which met the structural design requirements.

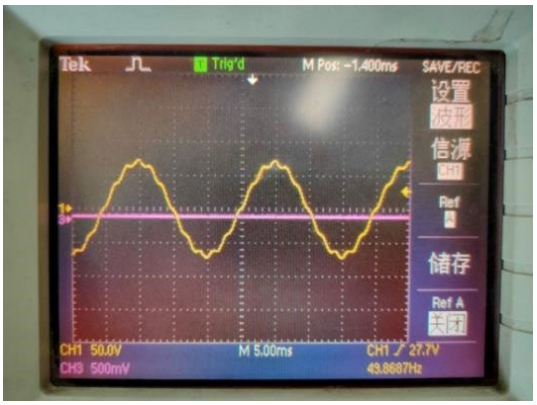

FIGURE 26. The measured back potential at 750rpm.

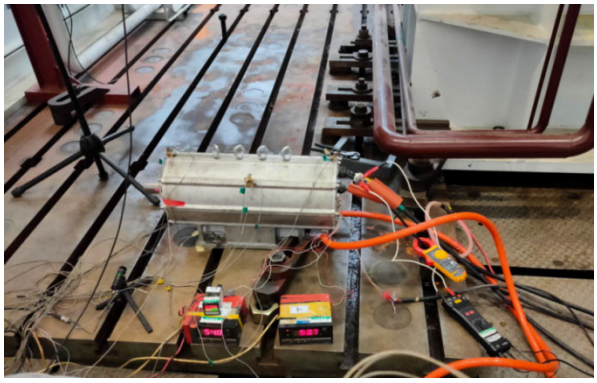

FIGURE 27. No-load test site.

FIGURE 28. Load test site.

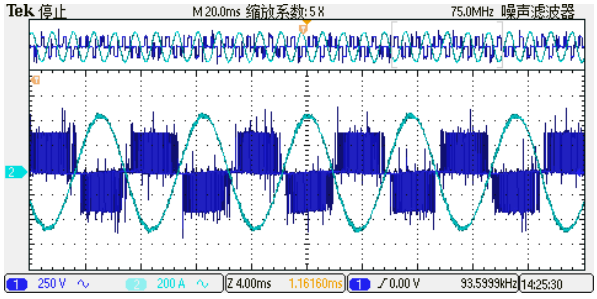

FIGURE 29. The measured voltage and current waveform at the speed of 2000rpm and the torque of 400Nm.

D. LOAD RUNNING TEST OF MOTOR

During the load test, due to the limitation of the existing gearbox load test conditions, the maximum speed can only reach 2000 rpm. Therefore, the performance of the permanent magnet motor under the remaining working conditions needs to be derived and verified according to the 2000 rpm load test data.

The motor was operated under no-load conditions using a variable frequency drive (VFD) until it reached a speed of 2000 rpm. Then, the load was gradually increased until the torque reached 400 Nm, and the on-site measured value was 405 Nm. The setup for the load test is illustrated in Figure 28, where a DC motor with a matching gearbox was used to provide different speeds and torques. The measured voltage and current waveforms at 2000 rpm are shown in Figure 29. Since PWM (Pulse Width Modulation) was used for power supply, the measured voltage appeared as a PWM square wave. After harmonic analysis, the corresponding line voltage amplitude was determined to be 160.6 V. Due to the filtering effect of the motor windings on high-frequency harmonic currents, the measured current appeared as a sine wave. After harmonic analysis, the current amplitude was determined to be 323 A. When converted to the rated speed, the voltage was found to be 345 V, which closely matched the design value of 350 V.

For 2400 rpm load conditions, according to the operating characteristic curve of the 180 kW permanent magnet motor, it mainly works in a constant torque state. The torque corresponding to the 2400 rpm load test condition is consistent with the torque (405 Nm) of the 2000 rpm load test above. It can therefore be deduced that the power corresponding to the load test 2400 rpm is 100 kW. Therefore, it can meet the power requirements of the propeller aerodynamic noise test platform for driving the motor to reach 100 kW at 2400 rpm.

For the 6500 rpm flux-weakening condition, according to the operating characteristic curve of the 180 kW permanent magnet motor, it mainly works in a constant power state, and the torque can reach 264.5 Nm to achieve the power requirement of 180 kW. For the motor rotor structure strength, the no-load operation test of 7000 rpm is carried out, and the rotor structure strength can meet the requirements. Therefore, it can meet the power requirements of the propeller aerodynamic noise test platform for driving the motor to reach 180 kW at 6500 rpm.

E. PROPELLER AERODYNAMIC NOISE TEST

The 180 kW permanent magnet motor is installed on the sliding platform of the test platform, as shown in Figure 30. The motor is driven by the inverter to rotate, and the propeller is driven by the main shaft. The axial pull force of the propeller is measured by the tension sensor at the back of the motor,

and the torque sensor on the main shaft is measured when the propeller is rotating. A condenser microphone is arranged in front of the propeller to measure the aerodynamic noise, so that the aerodynamic performance of the propeller such as tension, torque, power, and far-field noise directivity and spectrum characteristics can be studied.

The aerodynamic noise test of the full-size propeller was carried out in the semi-anechoic room, as shown in Figure 31. The propeller is made of composite material, the blade diameter is 1800 mm, and the propeller's maximum speed is 2400 rpm. The output power could be changed by adjusting the blade Angle. When the blade Angle is 15° and 27°, the measured results of the permanent magnet motor under various operating conditions are shown in Table 10 and Table 11. With the increase of the propeller speed, the output torque and power of the motor also increase. The end winding temperature of the motor is within the required temperature range, and the motor is in good running condition.

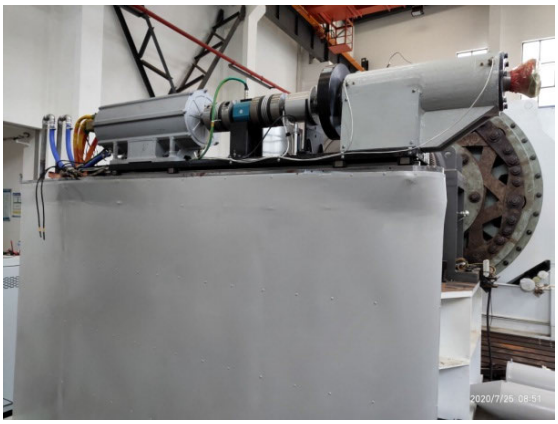

FIGURE 30. The structure composition of the propeller aerodynamic noise test platform.

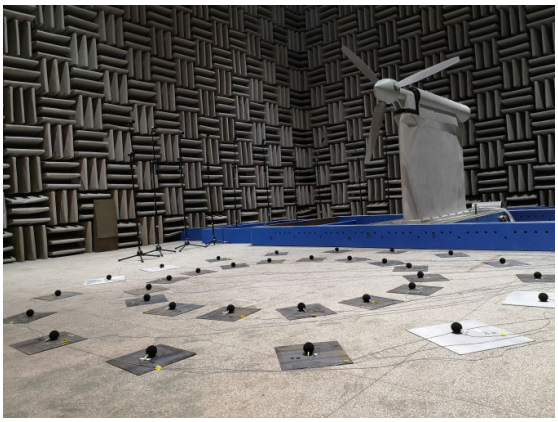

FIGURE 31. Propeller aerodynamic noise test.

The corresponding torque curve of the propeller under different speeds is shown in Figure 32, and its torque characteristic curve is parabolic. When the blade Angle is 27°, its output torque is larger, but because the maximum motor

TABLE 10. The measured data of 180 kW permanent magnet motor with blade Angle of 15°.

Speed/ rpm	Torque/ Nm	Power/ kW	Voltage/ V	Current /A	Temperature/ /°C
300	4.6	0.14	21	10	35.0
600	15.9	0.99	41	19	35.0
900	45.9	4.33	61	45	35.0
1200	77.0	9.75	81	78	35.1
1500	127.4	20.14	103	124	35.3
1600	141.1	23.80	114	140	35.8
1700	162.2	29.04	123	159	36.5
1800	182.7	34.63	132	175	37.4
1900	200.1	40.03	141	193	38.3
2000	227.4	47.87	152	214	39.4
2100	251.4	55.56	161	234	40.8
2200	279.8	64.75	171	259	42.3
2300	310.1	75.00	182	284	44.6
2400	349.7	88.26	196	315	50.5

TABLE 11. The measured data of 180 kW permanent magnet motor with blade Angle of 27°.

Speed/ rpm	Torque/ Nm	Power/ kW	Voltage/ V	Current /A	Temperature/ /°C
300	15.7	0.49	21	10	31
600	49.4	3.10	42	52	31
900	115.5	10.88	61	110	31
1200	200.4	25.18	90	181	32
1500	310.0	49.02	125	275	34
1600	356.5	59.73	134	311	41
1700	392.8	69.93	145	341	62

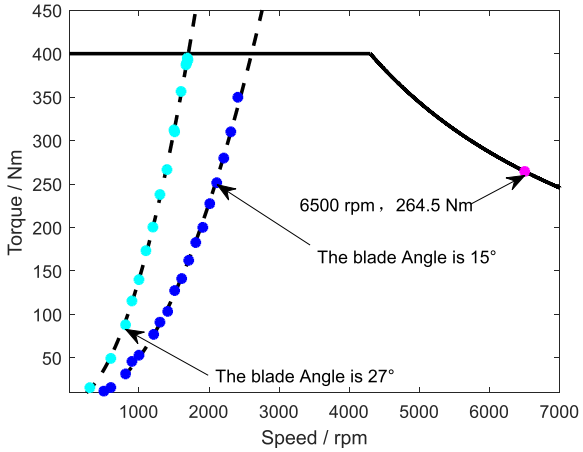

FIGURE 32. The measured results of the propeller aerodynamic noise test.

torque cannot exceed 400 Nm, the corresponding propeller speed cannot exceed 1700 rpm. When the blade Angle is 15°, its output torque is small, but because the maximum speed of the propeller cannot exceed 2400 rpm, the corresponding torque can only reach 349.7 Nm. It can be seen that when the blade Angle is 15° and the speed is 2400rpm, the measured torque value is 349.7 Nm and the measured power value is 88.2 kW. When the blade Angle is 27° and the speed is 1700 rpm, the measured torque value is 392.8 Nm and the measured power value is 69.9 kW. The drive motor runs smoothly on the test platform without abnormal vibration,

and the aerodynamic noise test of the full-size propeller has been successfully completed, and all requirements of the driving motor on the test platform have been met.

V. CONCLUSION

The aerodynamic noise test platform for a certain type of unmanned aerial vehicle sets stringent design requirements for the drive motor, including high torque, small outer diameter, and low vibration. These requirements pose higher demands and present certain design challenges for the motor. This paper provides a systematic exposition of the design methodology for a permanent magnet drive motor used in propeller aerodynamic noise testing, focusing on electromagnetic design, structural design, cooling design, and vibration design. Specifically, the core issue of electromagnetic design is elaborated in detail, covering aspects such as motor basic parameters and structure, motor modeling and equivalent boundary, no-load calculation, rated load calculation, weak magnetic calculation, and operating characteristic curve calculation. The results demonstrate that the motor meets the design requirements of 400 Nm torque and 100 kW power at 2400 rpm, as well as 264 Nm torque and 180 kW power at 6500 rpm. Under the rated and weak magnetic conditions, the maximum temperature of each part of the motor is 123.5 °C, satisfying the insulation requirements of Class H. The electromagnetic excitation frequency can avoid the blade frequency of the propeller under the main operating conditions. A 180 kW permanent magnet motor was successfully manufactured and used for propeller aerodynamic noise testing, meeting the technical requirements of the test platform for the drive motor.

This paper presents the design and fabrication of a 180 kW permanent magnet-driven motor, successfully used as the power drive for a propeller test platform. A rapid, efficient, and cost-effective test platform for the initial development of propellers was established in a semi-anechoic chamber, overcoming the high cost and size limitations associated with traditional wind tunnel testing. The paper comprehensively elaborates on the design methodology of permanent magnet-driven motors, covering electromagnetic design, structural design, cooling design, and vibration design. It emphasizes the importance of avoiding resonance between the electromagnetic excitation frequency of the motor and the radial modal frequencies of the stator structure and the blade frequency during vibration design. The proposed methodology was successfully applied in propeller aerodynamic noise testing, demonstrating its engineering application value. The findings can serve as a reference for the design of similar test platforms using permanent magnet-driven motors.

Based on the airworthiness standards specified by the Chinese civil aviation authorities [40], it can be inferred that the noise level of the propeller used in the unmanned aerial vehicle should be less than 70 dB(A). This sets a high bar for propeller design, and the paper will undertake further research on propeller noise reduction in subsequent work. Additionally, as propellers evolve towards higher speeds, the future research focus will be on developing permanent magnet direct-drive motors with higher speeds, larger power, smaller size, and lower vibration noise. The rotor dynamics design of the propeller shaft system is also a key technical challenge that requires considerable attention.

REFERENCES

[1] L. Wang, Q. Yan, D. W. Xue, and K. Wei, "Experimental investigation on noise reduction of double rotating propellers," *Equip. Environ. Eng.*, vol. 16, no. 7, pp. 18–22, Jul. 2019.

[2] D. W. Xue, X. Q. Liu, Q. Yan, and Y. H. Chen, "Joint optimization of aerodynamic and aeroacoustic for propeller blade," *Sci. Technol. Eng.*, vol. 22, no. 23, pp. 10310–10317, Aug. 2022.

[3] D. W. Xue, Q. Yan, Y. H. Chen, Z. H. Li, and K. Wei, "Multi-disciplinary design and experimental verification of low noise aircraft propellers," *J. Propuls. Technol.*, vol. 44, no. 7, pp. 1–10, Jul. 2023.

[4] B. J. Holmes, M. H. Durham, and S. E. Tarry, "Small aircraft transportation system concept and technologies," *J. Aircr.*, vol. 41, no. 1, pp. 26–35, Jan. 2004.

[5] K. Wei, Q. Cao, Q. Yan, J. Xu, and D. W. Xue, "Aerodynamic noise test of propeller of unmanned aerial vehicle," *Sci. Technol. Eng.*, vol. 23, no. 10, pp. 4426–4432, Oct. 2023.

[6] R. S. McKay, M. J. Kingan, S. T. Go, and J. Riul, "Experimental and analytical investigation of contra-rotating multi-rotor UAV propeller noise," *Appl. Acoust.*, vol. 177, Jun. 2021, Art. no. 107850.

[7] G. Sinibaldi and L. Marino, "Experimental analysis on the noise of propellers for small UAV," *Appl. Acoust.*, vol. 74, no. 1, pp. 79–88, Jan. 2013.

[8] D. Ciliberti and F. Nicolosi, "Design, analysis, and testing of a scaled propeller for an innovative regional turboprop aircraft," *Aerospace*, vol. 9, no. 5, p. 264, May 2022.

[9] G. Huo, Z. Wang, H. M. Kang, X. L. Liu, and J. Ye, "Development of high power density permanent magnet motor in FL-12 wind tunnel," *Ordnance Ind. Autom.*, vol. 40, no. 1, pp. 32–36, Jan. 2021.

[10] G. Huo, H. M. Kang, H. Li, X. L. Liu, and Y. Zhao, "Status and development direction of propeller test motor in wind tunnel," *Ordnance Ind. Autom.*, vol. 35, no. 11, pp. 20–23, Nov. 2016.

[11] Z. H. Hui, Y. Qiao, and Z. X. Zhu, "Research on high power density motor used f or wind tunnel test of propeller aerocraft model," *Micromotors*, vol. 39, no. 6, pp. 19–25, Jun. 2006.

[12] Z. X. Zhu, Z. H. Hui, and B. S. Wang, "Heating research on driven motor used in wind tunnel test of propeller aerocraft model," *Micromotors*, vol. 39, no. 1, pp. 52–54, Jan. 2006.

[13] H. Chen and C. H. T. Lee, "Parametric sensitivity analysis and design optimization of an interior permanent magnet synchronous motor," *IEEE Access*, vol. 7, pp. 159918–159929, 2019.

[14] Z. Chen and G. Li, "A V type permanent magnet motor simulation analysis and prototype test for electric vehicle," *IEEE Access*, vol. 7, pp. 174839–174846, 2019.

[15] S. Paul and J. Chang, "Fast model-based design of high performance permanent magnet machine for next generation electric propulsion for urban aerial vehicle application," *CES Trans. Electr. Mach. Syst.*, vol. 5, no. 2, pp. 143–151, Jun. 2021.

[16] X. X. Wu and L. Zhang, "Research on 80 kW high speed high power density permanent magnetic AC servo motor used in wind tunnel test of drive force," *Micromotors*, vol. 44, no. 1, pp. 14–16, Jan. 2011.

[17] G. Huo, H. M. Kang, X. L. Liu, Z. Wang, and F. Z. Chen, "Propeller driving force test system in FL-12 wind tunnel," *Ordnance Ind. Autom.*, vol. 37, no. 6, pp. 23–27, Jun. 2018.

[18] L. Y. Li, Y. Y. Guo, J. W. Cao, and B. P. Yan, "Research on the characteristic of electromagnetic-thermal of high speed and power density wind tunnel motor," *Electric Mach. Control*, vol. 17, no. 10, pp. 46–51, Oct. 2013.

[19] D. Duan, Z. Wang, Q. Wang, and J. Li, "Research on integrated optimization design method of high-efficiency motor propeller system for UAVs with multi-states," *IEEE Access*, vol. 8, pp. 165432–165443, 2020.

[20] Z. Hao, J. Shuanbao, W. Dong, W. Gongbao, and H. Pengfei, "Design and analysis of the integrated motor cooling system for shaftless propeller," *IEEE Access*, vol. 7, pp. 174573–174582, 2019.

[21] C. He and T. Wu, "Analysis and design of surface permanent magnet synchronous motor and generator," *CES Trans. Electr. Mach. Syst.*, vol. 3, no. 1, pp. 94–100, Mar. 2019.

[22] C. Liu, Y. Xu, J. Zou, G. Yu, and L. Zhuo, "Permanent magnet shape optimization method for PMSM air gap flux density harmonics reduction," *CES Trans. Electr. Mach. Syst.*, vol. 5, no. 4, pp. 284–290, Dec. 2021.
[23] F. Cui, Z. Sun, W. Xu, W. Zhou, and Y. Liu, "Comparative analysis of bilateral permanent magnet linear synchronous motors with different structures," *CES Trans. Electr. Mach. Syst.*, vol. 4, no. 2, pp. 142–150, Jun. 2020.
[24] D. Kim, J. Kim, H. Lim, J. Park, J. Han, and G. Lee, "A study on accurate initial rotor position offset detection for a permanent magnet synchronous motor under a no-load condition," *IEEE Access*, vol. 9, pp. 73662–73670, 2021.
[25] Y. Li, Y. Pang, J. Yang, and Y. Wang, "Structural expression code method and its application in optimal design of permanent magnet," *IEEE Access*, vol. 7, pp. 90517–90524, 2019.
[26] J. Liang, A. Parsapour, Z. Yang, C. Caicedo-Narvaez, M. Moallem, and B. Fahimi, "Optimization of air-gap profile in interior permanent-magnet synchronous motors for torque ripple mitigation," *IEEE Trans. Transport. Electrific.*, vol. 5, no. 1, pp. 118–125, Mar. 2019.
[27] S.-K. Cho, K.-H. Jung, and J.-Y. Choi, "Design optimization of interior permanent magnet synchronous motor for electric compressors of air-conditioning systems mounted on EVs and HEVs," *IEEE Trans. Magn.*, vol. 54, no. 11, pp. 1–5, Nov. 2018.
[28] H.-S. Chen, D. G. Dorrell, and M.-C. Tsai, "Design and operation of interior permanent-magnet motors with two axial segments and high rotor saliency," *IEEE Trans. Magn.*, vol. 46, no. 9, pp. 3664–3675, Sep. 2010.
[29] S. Lee, K. Kim, S. Cho, J. Jang, T. Lee, and J. Hong, "Optimal design of interior permanent magnet synchronous motor considering the manufacturing tolerances using Taguchi robust design," *IET Electric Power Appl.*, vol. 8, no. 1, pp. 23–28, Jan. 2014.
[30] M. K. Yoon, C. S. Jeon, and S. K. Kauh, "Efficiency increase of an induction motor by improving cooling performance," *IEEE Trans. Energy Convers.*, vol. 17, no. 1, pp. 1–6, Mar. 2002.
[31] Z. Huang, J. Fang, X. Liu, and B. Han, "Loss calculation and thermal analysis of rotors supported by active magnetic bearings for high-speed permanent-magnet electrical machines," *IEEE Trans. Ind. Electron.*, vol. 63, no. 4, pp. 2027–2035, Apr. 2016.
[32] X. Fan, R. Qu, J. Li, D. Li, B. Zhang, and C. Wang, "Ventilation and thermal improvement of radial forced air-cooled FSCW permanent magnet synchronous wind generators," *IEEE Trans. Ind. Appl.*, vol. 53, no. 4, pp. 3447–3456, Jul. 2017.
[33] A. Boglietti, A. Cavagnino, D. Staton, M. Shanel, M. Mueller, and C. Mejuto, "Evolution and modern approaches for thermal analysis of electrical machines," *IEEE Trans. Ind. Electron.*, vol. 56, no. 3, pp. 871–882, Mar. 2009.
[34] H. Yang and Y. Chen, "Influence of radial force harmonics with low mode number on electromagnetic vibration of PMSM," *IEEE Trans. Energy Convers.*, vol. 29, no. 1, pp. 38–45, Mar. 2014.
[35] G. Verez, G. Barakat, Y. Amara, and G. Hoblos, "Impact of pole and slot combination on vibrations and noise of electromagnetic origins in permanent magnet synchronous motors," *IEEE Trans. Magn.*, vol. 51, no. 3, pp. 1–4, Mar. 2015.
[36] H. Yu, Z. Lu, L. Sun, and Y. Zhou, "Characterization of the structural vibration response of the driven motor used for propeller systems," in *Proc. IEEE 6th Int. Electr. Energy Conf. (CIEEC)*, May 2023, pp. 2626–2630.
[37] H. Yu, L. Tian, and G. Zhang, "Transfer path analysis of structural vibration on propulsion motor," *IEEE Trans. Magn.*, vol. 51, no. 11, pp. 1–3, Nov. 2015.
[38] R. Y. Tang, "The basis of magnetic circuit calculation of permanent magnet motor," in *Modern Permanent Magnet Machines: Theory and Design*, 1st ed. Beijing, China: China Machine Press, 1997, pp. 88–92.
[39] S. K. Chen, "Magnetic circuit calculation," in *Design of Electrical Motor*, 1st ed. Beijing, China: China Machine Press, 2000, pp. 60–63.
[40] *Aeroengine Airworthiness Regulations*, CCAR-36, Civil Aviation Admin. China, Beijing, 2022.

HU YU received the B.S. and Ph.D. degrees in environmental acoustics from Northwestern Polytechnical University, China, in 2004 and 2013, respectively. In 2013, he joined the Wuhan Institute of Marine Electric Propulsion, Wuhan, China, and worked on the design and analysis of special electric machines, especially the permanent magnet synchronous motor. His research interests include vibration and noise control, and the structural design of electric machines.

YONG-HUI CHEN graduated from Northwestern Polytechnical University, in 2011. He is currently with the Aeronautical Strength Research Institute, mainly researching vibration and noise control technology for aircraft engines.

LIANG SUN received the B.S. degree in mechanical engineering from the Shandong University of Architecture, in 2003, and the Ph.D. degree from Northwestern Polytechnical University, in 2010. In 2013, he was a Research Associate with the Department of Physics, The Hong Kong University of Science and Technology, Hong Kong, where he has been a Research Assistant Professor, since 2015. In 2022, he joined the City University of Hong Kong. His research interests include acoustic metamaterials and low-frequency vibration attenuation by resorting to acoustic metamaterials.

YONG ZHOU received the B.S. and M.S. degrees in marine engineering from the Wuhan University of Technology, China, in 2004 and 2007, respectively. In 2007, he joined the Wuhan Institute of Marine Electric Propulsion, Wuhan, China, and worked on the design and analysis of special electric machines, especially the high-temperature superconducting motor and high-speed permanent magnet synchronous motor with high power density. His research interests include vibration and noise control, composite material design, and the structural design of electric machines.

ZHONG-REN WANG received the B.S. degree from the Beijing University of Chemical Technology, China, in 1997, and the M.S. degree and the Ph.D. degree in mechanical engineering from the South China University of Technology, Guangzhou, in 2003 and 2009, respectively. Since 2003, he has been with the School of Mechanical Engineering, Hubei University of Arts and Science. He is currently a Professor and the Leader of the Key Laboratory of Intelligent Manufacturing and Machine Vision. His current research interests include machine vision, machine hearing, machine learning, and intelligent welding.